

# Modeling aqueous-phase hydrodeoxygenation of sorbitol over Pt/SiO<sub>2</sub>-Al<sub>2</sub>O<sub>3</sub><sup>†</sup>

Cite this: *RSC Adv.*, 2013, **3**, 23769

Brian M. Moreno,<sup>a</sup> Ning Li,<sup>‡b</sup> Jechan Lee,<sup>§b</sup> George W. Huber<sup>§\*b</sup>  
and Michael T. Klein<sup>\*a</sup>

In this paper, we investigated the effects of temperature, hydrogen partial pressure, and sorbitol concentration on the aqueous-phase hydrodeoxygenation (APHDO) of sorbitol over a bifunctional 4 wt % Pt/SiO<sub>2</sub>-Al<sub>2</sub>O<sub>3</sub> catalyst in a trickle bed reactor. APHDO involves four fundamental reactions: (1) hydrogenation; (2) dehydration; (3) C-C bond cleavage by dehydrogenation and decarbonylation; and (4) C-C bond cleavage by dehydrogenation and retro-aldol condensation. The main deoxygenation routes are decarbonylation and alcohol dehydration. Retro-aldol condensation plays a critical role in reducing the carbon number of the products. The key products in this system are C1-C6 *n*-alkanes, primary and secondary alcohols, and carbon dioxide. As shown in this paper, the reaction conditions can dramatically change the product selectivity for APHDO of biomass-derived feedstocks (e.g., sorbitol). A sorbitol hydrodeoxygenation reaction network was generated that predicts all of the 43 experimentally measured species. The reaction network consists of 4804 reactions and produces a total of 1178 distinct chemical species. The associated material balance equations were solved numerically to model the experimentally observed species as a function of temperature, concentration, and pressure. The model concentrations fit well the experimentally measured values, demonstrating that the model was accurately able to model the reaction families and capture the salient features of the experimental observations. The trend observed in this paper can be used for the optimization of reactors and new catalysts to selectively make targeted products by hydrodeoxygenation of biomass-derived feedstocks.

Received 17th September 2013  
Accepted 25th September 2013

DOI: 10.1039/c3ra45179h

[www.rsc.org/advances](http://www.rsc.org/advances)

## 1. Introduction

The sustainable production of liquid fuels and chemicals from biomass has attracted much attention as an alternative to fossil fuels because of the availability and low cost of lignocellulosic biomass.<sup>1-6</sup> Biomass feedstocks have a high number of highly reactive organic functional groups. Biomass conversion involves selective removal of oxygen from the biomass.<sup>6-8</sup> The biomass feedstock reacts with hydrogen *via* aqueous-phase hydrodeoxygenation (APHDO) to produce alkanes, alcohols, and polyols.<sup>9-22</sup> Bifunctional catalyst systems are typically used for APHDO reactions and involve metal<sup>23,24</sup> and acid sites.<sup>13-25</sup> Sorbitol has previously been used as a model compound to study the HDO of biomass.<sup>14,16,26</sup>

During sorbitol conversion, oxygen is removed by two different pathways: (1) alcohol dehydration (removal of hydroxyl groups as water primarily on acid catalytic sites) and (2) decarbonylation (removal of aldehyde groups as carbon monoxide primarily on metal catalytic sites).<sup>27,28</sup> Hydrogen then reacts with the C=C and C=O bonds generated during alcohol dehydration to produce a saturated compound. The dehydration route is advantageous compared to decarbonylation because no carbon from the biomass is lost in this process. However, the dehydration route does consume large amounts of hydrogen, and produces very large quantities of water.<sup>29</sup>

A schematic network of the reaction families for HDO of sorbitol is presented in Fig. 1. The reactions that occur during this process include alcohol dehydration, cyclization, dehydrogenation, decarbonylation, hydrogenolysis, and retro-aldol condensation. Measured products are produced by a stepwise combination of these reaction pathways, as indicated in the figure. Furan and pyran species are produced *via* cyclization of C4-C6 alcohols, followed by numerous dehydration and cracking reactions. Several of the smaller species are produced *via* retro-aldol condensation. The carbon monoxide produced from decarbonylation is converted to carbon dioxide *via* the water-gas shift reaction.

<sup>a</sup>Department of Chemical and Biomolecular Engineering, University of Delaware, 150 Academy Street, Newark, DE 19716, USA. E-mail: [mtk@udel.edu](mailto:mtk@udel.edu)

<sup>b</sup>Department of Chemical Engineering, University of Massachusetts Amherst, 686 North Pleasant Street, Amherst, MA 01003, USA

<sup>†</sup> Electronic supplementary information (ESI) available. See DOI: 10.1039/c3ra45179h

<sup>‡</sup> Current address: Dalian Institute of Chemical Physics, Chinese Academy of Sciences, Dalian 116023, China.

<sup>§</sup> Current address: Department of Chemical and Biological Engineering, University of Wisconsin-Madison, 1415 Engineering Drive, Madison, WI 53706, USA.

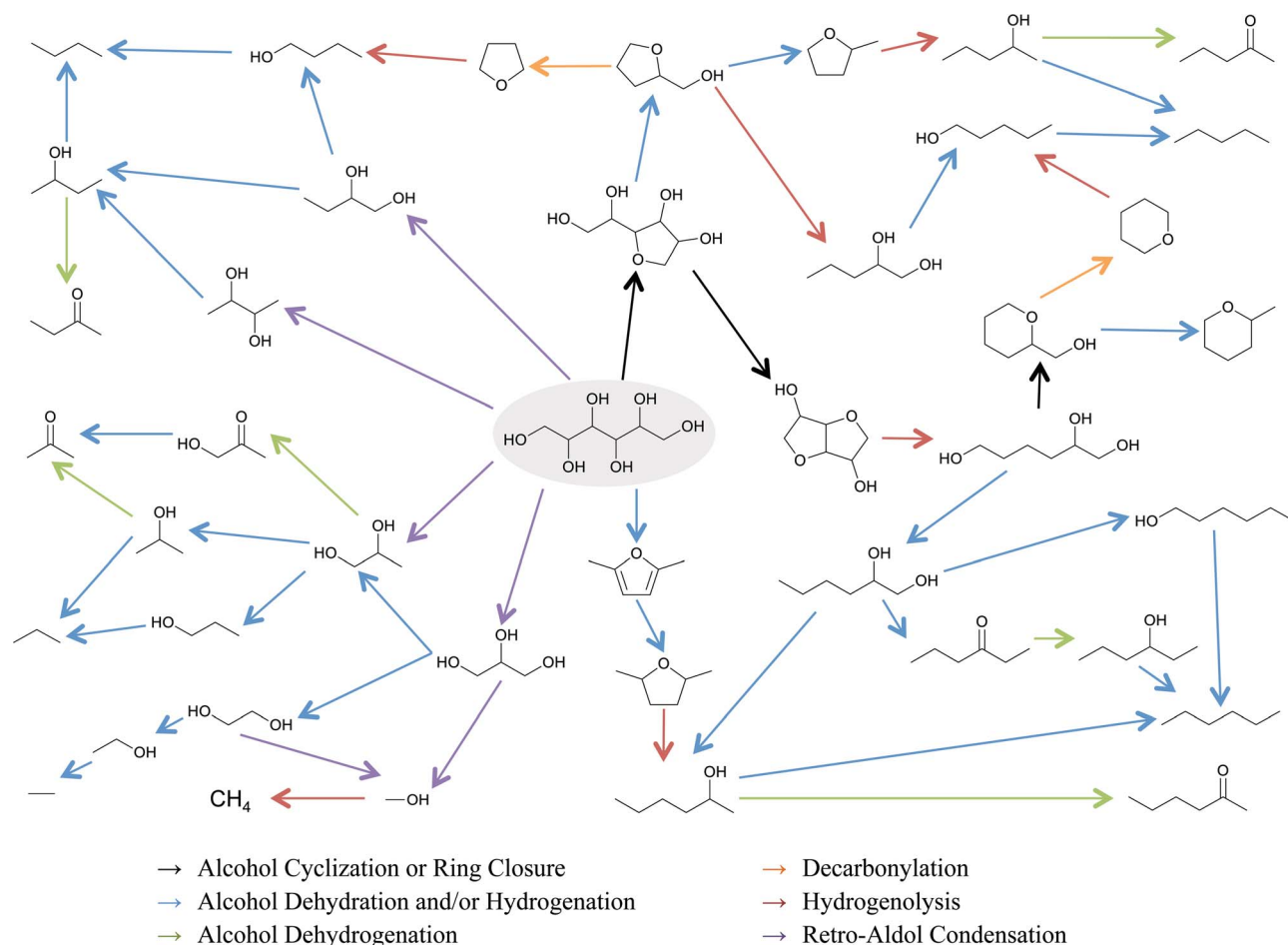


**Fig. 1** Major reaction pathways for aqueous-phase hydrodeoxygenation (APHDO) of sorbitol.

While there has been a tremendous interest in using HDO reactions to convert biomass into fuels and chemicals, there has been no kinetic study done for HDO. The objective of this paper is to develop a kinetic model for HDO of sorbitol that can describe the complicated products that are produced in this process. Molecular-level kinetic models preserve the identities of each species within a chemical system. Since the species produced during biomass conversion are not as well documented as those produced from traditional petroleum fuels, molecular-level models are very helpful to identify reaction intermediates. With these specific molecular identities, it is possible to predict the physical properties of the novel oxygenate species in biomass pyrolysis oils and deoxygenated products. Furthermore, the kinetic rates of each deoxygenation pathway could direct research for the design of improved catalysts as well as help to identify the reaction conditions that will make biofuels a competitive energy source.

## 2. Experimental methods

### 2.1. Catalyst preparation

The  $\text{SiO}_2\text{-Al}_2\text{O}_3$  (SIAL3125,  $\text{SiO}_2\text{-Al}_2\text{O}_3$  molar ratio about 4.0) support was supplied by Grace Davison. The platinum was

loaded on different supports by incipient wetness impregnation with *tetra*-amine platinum nitrate (Strem Chemicals) aqueous solution according to literature.<sup>9,10</sup> The platinum content in the catalyst was 4 wt%. The mixture was then dried in an oven overnight at 373 K and calcined at 533 K for 3 h in air. The BET surface area of the  $\text{Pt/SiO}_2\text{-Al}_2\text{O}_3$  as prepared was measured as  $430 \text{ m}^2 \text{ g}^{-1}$  by nitrogen adsorption at 77 K using a Quantchrome Autosorb Automated Gas Sorption System. From the hydrogen chemisorption experiment carried out at 303 K on the same instrument, the catalysts had a hydrogen uptake of  $74.25 \mu\text{mol H}_2 \text{ g}_{\text{catalyst}}^{-1}$ , which corresponds to an H to Pt ratio of 0.724.

### 2.2. Catalyst test

The hydrodeoxygenation experiments were carried out in a stainless steel tubular flow reactor heated by a Lindberg (type 54032) furnace. In order to ensure a uniform temperature profile along the catalyst bed, an aluminum tube was split lengthwise and was inserted in the void between the heating tube of the furnace and tubular reactor. Subsequently, it was found that the temperature difference between the middle and top of the tubular reactor was less than 15 K.

Prior to the reaction, the Pt/SiO<sub>2</sub>-Al<sub>2</sub>O<sub>3</sub> was reduced in the reactor with hydrogen flowing from the bottom at approximately 200 mL min<sup>-1</sup>. The reduction temperature of the Pt/SiO<sub>2</sub>-Al<sub>2</sub>O<sub>3</sub> catalyst increased from room temperature to 723 K at 50 K h<sup>-1</sup> and was then held at 723 K for 2 h. The reactor was then cooled down to the reaction temperature and the pressure was slowly increased to the desired value.

The liquid feed (5 wt% sorbitol aqueous solution) was co-fed with hydrogen (45 mL min<sup>-1</sup>) through the catalyst from the bottom of reactor with the help of a JASCO PU980 HPLC pump. A gas-liquid separator was utilized downstream of the reactor tube. The gaseous products from the reactor flowed through a backpressure regulator, used to maintain the pressure of the reaction system.

The gaseous products were further analyzed by two online gas chromatographs (HP 5890 series II). Carbon dioxide in the gaseous product was analyzed by a Thermal Conductivity Detector (TCD) in conjunction with an Alltech HAYESEP DB 100/120 packed column (Part no. 2836PC) that was heated at a constant temperature (348 K). The TCD and the injection port were held at 433 K and at 393 K, respectively. The column flow rate was 41 mL min<sup>-1</sup> with helium as the carrier gas.

Alkanes in the gaseous product were analyzed with a flame ion detector (FID) with an Alltech AT-Q capillary column (30 m, 0.32 mm I.D., Part no. 13950). Helium was used as the carrier gas with a column flow rate of 1 mL min<sup>-1</sup>. Both the injection port and the detector were held at 473 K. The split ratio was 100. The GC oven temperature was held at 313 K for 6 min, ramped to 453 K at 5 K min<sup>-1</sup>, and held at 453 K for 25 min.

Liquid product that accumulated in the gas-liquid separator was drained periodically and analyzed by GC-MS and HPLC. The GC-MS is Shimadzu GC-2010 with an Rtx-VMS capillary column (30 m, 0.25 mm I.D., film thickness 1.4 μm). Helium was used as the carrier gas with a column flow rate of 1.57 mL min<sup>-1</sup>. Both the injection port and the detector were held at 513 K. For each analysis, a 1 μL liquid sample was injected with a split ratio of 200. The column was held at 308 K for 5 min, ramped to 323 K at 5 K min<sup>-1</sup>, then to 513 K at 20 K min<sup>-1</sup>, and kept at 513 K for 7.5 min. A Shimadzu HPLC with UV-Vis (SPD-20AV) and RID (RID-10A) detectors was also used to analyze the liquid products. A 1 μL liquid sample was injected for each sample. The products were separated by a BIO-RAD Aminex HPX-87H column (Catalog no. 125-0140) that was maintained at 303 K with 0.005 M H<sub>2</sub>SO<sub>4</sub> as the mobile phase flowing at a rate of 0.6 mL min<sup>-1</sup>.

Finally, a total organic carbon (TOC) analyzer (Shimadzu TOC-5000A) was used to check the carbon balance. The liquid sample was taken at least 12 h after the reaction conditions were changed when the gas phase results were constant. From the GC analysis results, reaction equilibrium was reached within 8 h.

To exclude the effect of deactivation of the catalyst, we checked the stability of the catalyst under each reaction condition. No evident change of activity or selectivity of the catalyst was observed after a continuous run of 24 h, indicating that the catalyst is stable under the conditions used in this paper. There was no coking on the catalyst under the reaction conditions we used in this process.

### 3. Modeling methods

#### 3.1. Generation of reaction network *via* INGen

The Klein research group has enabled automated network generation for biomass pyrolysis and subsequent hydrodeoxygenation through the development of INGen, the Interactive Network Generator.<sup>30</sup> User-selected seed molecules and allowable reaction types determine the size and complexity of the reaction network.

INGen combines relevant mechanistically informed reaction pathways to completely describe the reactivity of a given chemical system. The intuitive interface allows a user to select reaction types and seed molecules to initialize the reaction network. INGen then automatically generates an exhaustive reaction network by searching for reactable moieties within each molecule and writing all possible reactions. Performing this kind of search on a computer requires the computational definition of a chemical species as well as a way to transform those reactant species into distinct products.

Chemical species are computationally defined in INGen using bond electron matrices, which are intuitive representations of the atoms and their corresponding bond connections within molecules. Each element of a bond electron matrix indicates the formal bond order between any given pair of atoms in a molecule. A large library of preexisting species is included with INGen, and new species may be added by simply sketching the molecule in ChemDraw and converting to the appropriate file type.

Given the bond electron matrix representation of a reactant molecule, it becomes apparent that the addition and subtraction of bonds within that matrix represents the breaking and forming of bonds in a chemical reaction. INGen writes chemical reactions by applying reaction matrices for each reaction family to all of the reactable moieties within each chemical species. A reactant matrix is converted into a different product matrix during each chemical reaction.

For each reaction family in this model, the reaction matrix is given along with a sample reactant and product matrix pair in Fig. 2. The reactive atomic sites are listed in a particular order to standardize the reaction operator for that reaction family. A reaction is defined by three properties: the site neighborhood, the reaction site, and the reaction operator.

The site neighborhood is the connectivity of atoms that is required to participate in a given reaction type, although all of the atoms within the site neighborhood do not necessarily change connectivity during the reaction. Site neighborhoods are most closely analogous to chemical moieties, such as the hydroxyl group in the reactant depicted in Fig. 2b. The reaction site itself defines which atoms will participate in the reaction, and the order in which they will be acted upon. These are the atoms whose connectivities will change during the reaction. The reaction operator (the reaction matrix specific to the reaction family) defines how to affect the bonds of the site atoms. Generally, only a small number of atoms and bonds are modified in a given chemical reaction.

To exemplify each of the site selection aspects of automated network generation, we may continue to focus on the alcohol

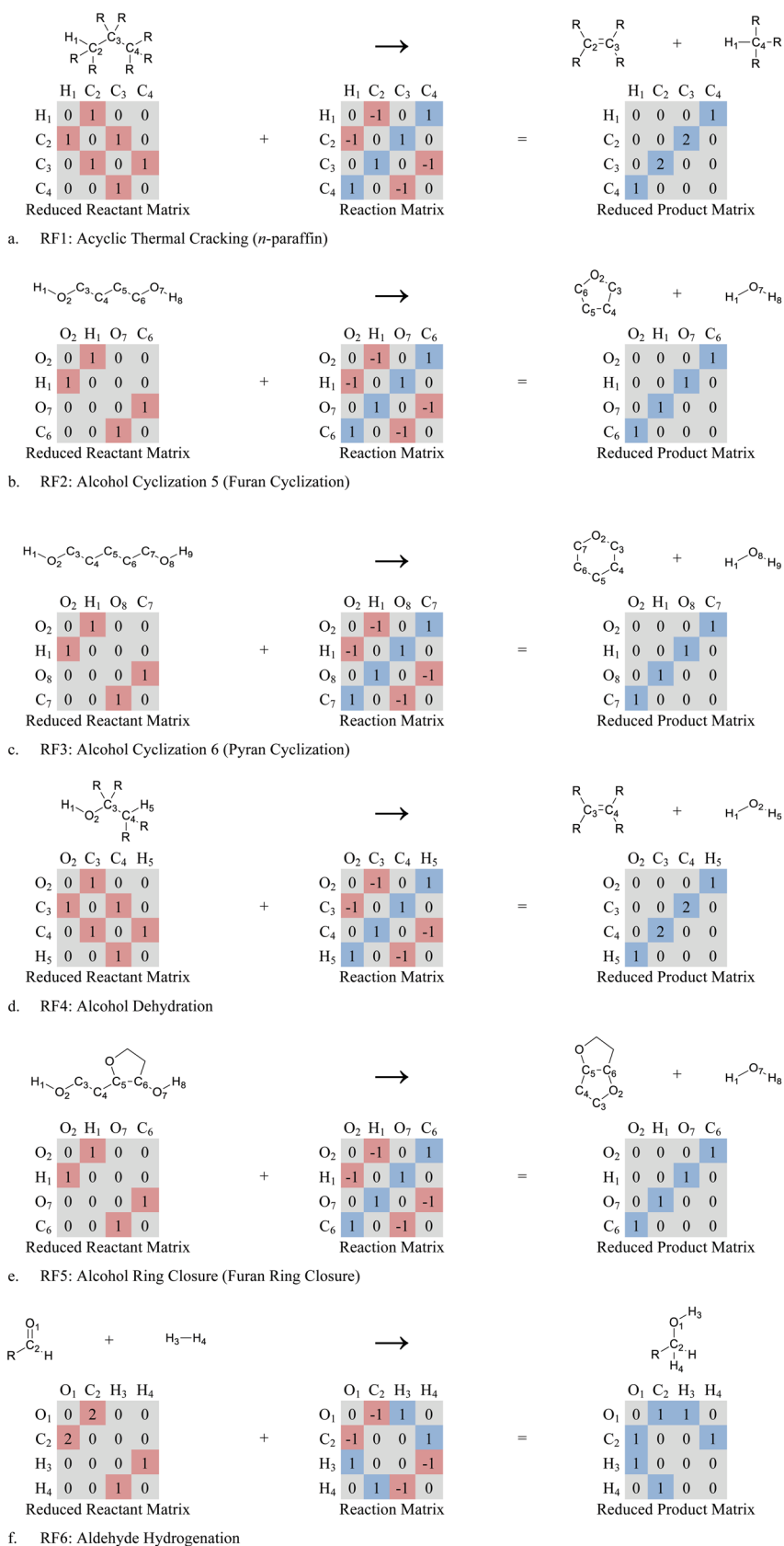
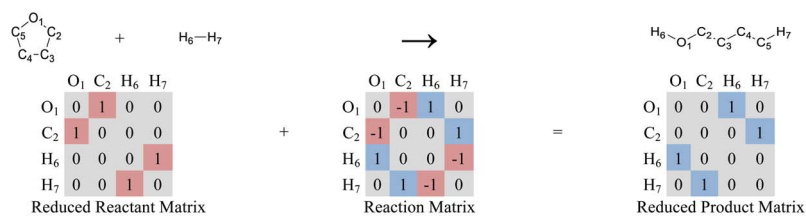
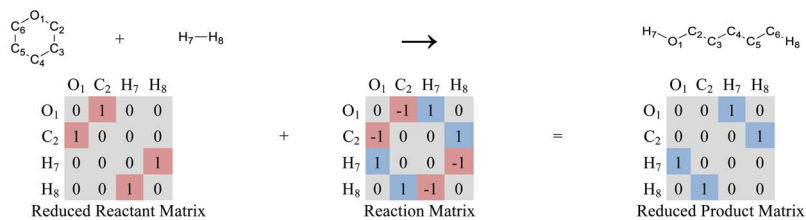


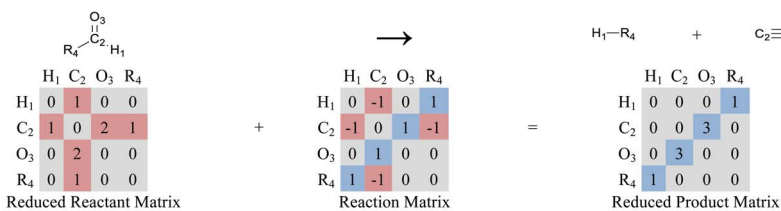
Fig. 2 (Contd.)



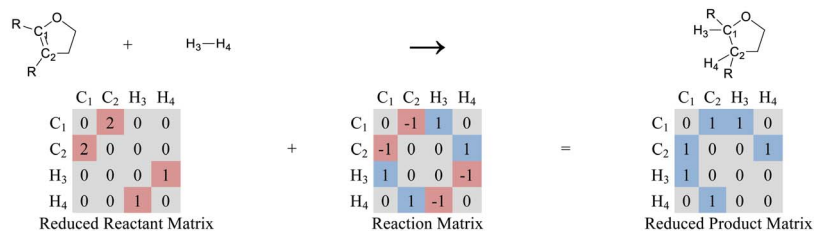
g. RF7: C-O Hydrogenolysis 5 (Furan Ring Opening)



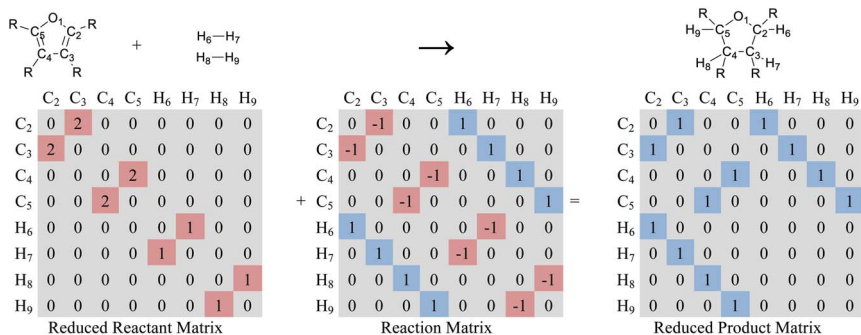
h. RF8: C-O Hydrogenolysis 6 (Pyran Ring Opening)



i. RF9: Decarbonylation



j. RF10: Furan Ring Saturation 2H



k. RF11: Furan Ring Saturation 4H

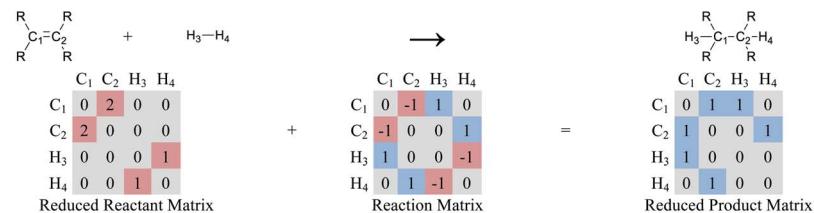
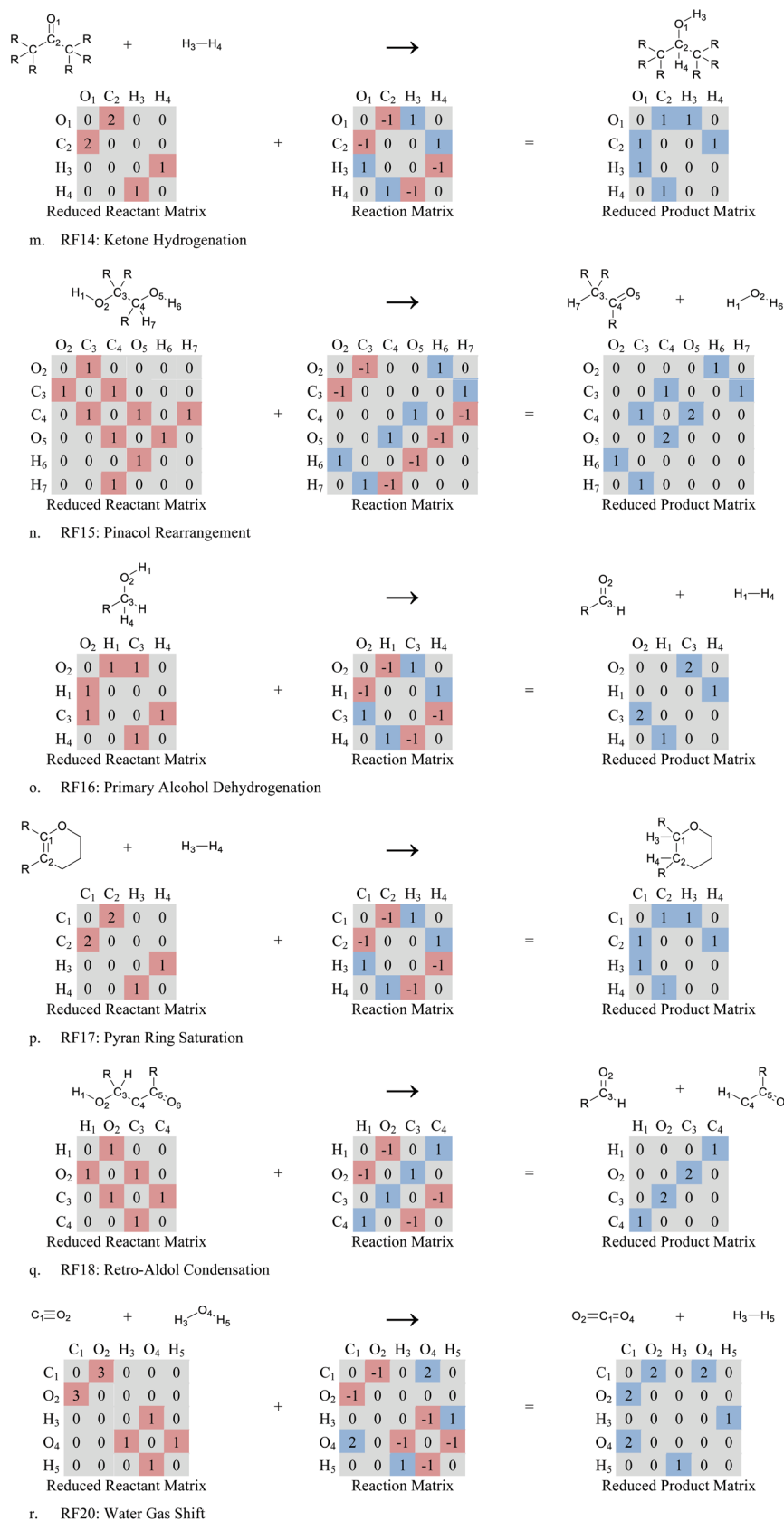
l. RF12 & RF13: Hydrogenation (*n*-olefin & oxygenated species)

Fig. 2 (Contd.)



**Fig. 2** Chemical reactions as matrix operations. In most cases, R groups on carbon atoms are implicit if they do not directly participate in the reaction.

cyclization reaction depicted in Fig. 2b. We must first locate a specific sequence of atoms: H<sub>1</sub>–O<sub>2</sub>–C<sub>3</sub>–C<sub>4</sub>–C<sub>5</sub>–C<sub>6</sub>–O<sub>7</sub>–H<sub>8</sub>. The reaction occurs when the reaction matrix is added to the reactant matrix, which breaks and forms chemical bonds and gives the product species. A single bond electron matrix temporarily represents the two product species. This process of adding reaction matrices to appropriately selected reactant matrices leads to the generation of a complete reaction network for the given chemical system.

Pinacol rearrangement (Fig. 2n) is a particularly interesting reaction family in this model. The overall reaction in a pinacol rearrangement produces water and a carbonyl (aldehyde or ketone).<sup>31,32</sup> This reaction family specifically affects pairs of hydroxyl groups on adjacent carbon atoms in which traditional alcohol dehydration would have resulted in an unstable enol (carbon–carbon double bond with an adjacent hydroxyl group). Sorbitol and its products contain many adjacent hydroxyl groups that undergo pinacol rearrangements.

All reactions were written irreversibly to simplify the model and shorten the solution time. When applicable, reverse reactions were written separately.

### 3.2. Tuning of kinetic parameters via KME

This chemical system was modeled as a PFR with 3.3 g of Pt/SiO<sub>2</sub>–Al<sub>2</sub>O<sub>3</sub> catalyst at a loading density of 1.26 g cm<sup>–3</sup>, resulting in reactor dimensions of 0.246 cm in diameter and 54.9 cm in length. Molar flow rates for positional isomers were divided according to the percentages in Table 8 (ESI†).

From the completed reaction network, all of the mass balances are automatically generated and subsequently solved numerically by KME (the Kinetic Modeling Editor).<sup>33</sup> Kinetic rate parameters were tuned using the data sets that had 100–105 mol% carbon identified with identical sorbitol feed concentration of 5 wt%, temperature of 518 K, and weighted hourly space velocity (WHSV) of 0.73 h<sup>–1</sup>, where the pressure varied between 2.93 and 4.90 MPa (data sets 2, 8, 9, and 10). Kinetic parameter tuning was performed using simulated annealing of a least squares optimization function, *F* (minimization of the sum of squares of residuals), via KME.

The adjustable parameters in this kinetic model are given in eqn (1) and (2). The Arrhenius expression for the rate constant, *k<sub>j</sub>*, identifies the pre-exponential factor, *k<sub>0,i</sub>*, and the activation energy, *E<sub>j</sub><sup>\*</sup>*, for each reaction, *j*.

$$\log k_j = \log k_{0,i} - E_j^*/2.303RT \quad (1)$$

The Evans–Polanyi linear free energy relationship (LFER)<sup>34</sup> given in eqn (2) allows for differences in the rate constants of individual reactions (*j*) within reaction families (*i*). These differences result from the enthalpy change of each reaction, which leads to faster kinetic rates for energetically favored reactions. *E<sub>j</sub><sup>\*</sup>*, the activation energy of reaction *j*, is a function of *E<sub>0,i</sub><sup>\*</sup>*, the activation energy of reaction family *i* (set to zero), *α<sub>i</sub>*, the LFER constant of reaction family *i* (tuned by KME), and *ΔH<sub>R,j</sub>*, the enthalpy change of reaction *j* (calculated by group contribution methods via CME).<sup>35</sup> The LFER constant indicates the

extent to which individual reactions within a given reaction family depend upon their unique energy barrier ( $-1 \leq \alpha_i \leq 1$ ).

$$E_j^* = E_{0,i}^* + \alpha_i \Delta H_{R,j} \quad (2)$$

An example of this relationship is the hydrogenation of hexa-1,3-diene to hex-1-ene (Reaction 2402) and hex-3-ene (Reaction 2403), in which the hydrogenation of the secondary alkene is more energetically favorable than the hydrogenation of the primary alkene ( $\Delta H_{R,2402} < \Delta H_{R,2403}$ ). Therefore, although both of these reactions are members of the same reaction family, the rate constant for the hydrogenation of the secondary alkene is larger ( $k_{2402} > k_{2403}$ ).

The enthalpy change for each of the 4804 reactions is available as ESI (Table 9).† To simplify parameter tuning and to account for the identical reaction temperature of tuned data sets, *E<sub>0,i</sub><sup>\*</sup>* was set to zero for each reaction family. Thus, the only tuned parameters in this kinetic model are log *k<sub>0,i</sub>* and *α<sub>i</sub>* for each of the 20 reaction families, resulting in a total of 40 tuned kinetic parameters.

## 4. Results

### 4.1. Aqueous-phase hydrodeoxygenation of sorbitol

**4.1.1. Effects of reaction temperature.** We investigated the effect of reaction temperature on the catalytic performance of the 4 wt% Pt/SiO<sub>2</sub>–Al<sub>2</sub>O<sub>3</sub> at weight hourly space velocities (WHSV) of 0.73 h<sup>–1</sup> and 2.91 h<sup>–1</sup> as shown in Table 1. The gas products were composed of CO<sub>2</sub> and C1–C6 straight-chain alkanes. We did not detect any CO in the gas phase. The liquid phase products included alcohols, diols, polyols, ketones, cyclic ethers, 1,4-sorbitan, isosorbide, and unconverted sorbitol. We were able to quantify between 76 and 100 mol% of the products in Table 1. The carbon balances were occasionally low as a result of some unidentified species that were not reported.

The gas phase yield increases with reaction temperature. A lower CO<sub>2</sub> gas phase selectivity (C–C bond cleavage) and higher alkane selectivity (C–O bond cleavage) is observed at low WHSV and/or high temperature. The specific gas phase selectivities of C1–C6 alkanes were very similar.

The C1 liquid phase selectivity increased with reaction temperature at WHSV = 2.91 h<sup>–1</sup>. The C2–C3 selectivity went through a maximum at low WHSV. This same fraction increased with temperature at high WHSV. The C1–C3 products were mainly composed of methanol, ethanol, propanol, propane-1,2-diol, and glycerol.

The selectivity of C4 in the liquid phase decreased with temperature at low WHSV and increased with temperature at high WHSV. At high space velocity (WHSV = 2.91 h<sup>–1</sup>), the selectivity of C6 compounds decreased with reaction temperature (higher reaction rate at high temperature), while the C1–C5 selectivity increased.

**4.1.2. Effects of system pressure.** We also investigated the effect of system pressure for the APHDO of 5 wt% sorbitol solution over the Pt/SiO<sub>2</sub>–Al<sub>2</sub>O<sub>3</sub> catalyst as shown in Table 2. As total pressure increased, the initial concentration of hydrogen and sorbitol at the reactor inlet increased. The carbon

**Table 1** Total molar carbon selectivity of products in gas- and liquid-phase as a function of temperature for the APDO of sorbitol<sup>a</sup>

Data set number	1	2	3	4	5	6	
WHSV (h <sup>-1</sup> )	0.73	0.73	0.73	2.91	2.91	2.91	
Temperature (K)	498	518	538	498	518	538	
Conversion (mol%)	100	100	100	74.6	100	100	
Gas phase yield (mol%)	37.8	80.8	85.3	10.8	39.7	71.5	
<b>Gas phase carbon selectivity (mol%)</b>							
C1	Carbon dioxide	59.9	40.4	41.0	90.1	62.6	51.5
	Methane	5.2	5.2	5.9	0.6	5.4	5.0
C2	Ethane	10.1	13.8	14.8	1.2	9.0	11.7
C3	Propane	7.5	9.7	9.9	1.2	6.6	7.3
C4	Butane	7.1	10.4	10.7	1.2	6.5	8.2
C5	Pentane	5.3	8.9	8.6	2.2	5.7	8.0
C6	Hexane	4.9	11.6	9.1	3.6	4.2	8.3
<b>Liquid phase yield (mol%)</b>							
C1		1.5	2.1	1.2	0.3	1.1	1.4
C2		7.3	5.7	2.6	1.4	1.2	2.9
C3		11.9	8.8	3.9	5.9	7.0	4.9
C4		4.1	1.0	0.7	0.5	1.7	2.5
C5		10.4	1.9	4.0	8.0	10.0	8.3
C6		11.4	1.4	6.6	50.6	15.3	7.0
<b>Liquid phase carbon selectivity (mol%)</b>							
C1	Methanol	3.3	9.9	6.2	0.4	2.9	5.1
C2	Ethanol	15.6	27.5	13.5	2.1	3.3	10.7
C3	Propanol	16.0	40.3	17.7	1.1	7.4	13.1
	Acetone	0.9	0.9	1.0	0.2	2.1	2.8
	Glycol	0	0	0	0	0	0
	Propane-1,2-diol	8.5	1.0	1.7	3.6	9.8	2.5
	1-Hydroxypropan-2-one	0	0	0	0	0	0
	Glycerol	0	0	0	4.0	0	0
C4	Butanol	4.5	4.6	1.6	0.5	0.9	3.8
	Butanone	0	0	2.0	0.2	2.3	5.3
	Tetrahydrofuran	0	0	0	0	0	0
	Butanediol	4.3	0	0	0	1.6	0
C5	Pentanol	3.9	0.8	4.9	0.3	4.0	3.3
	Pentanone	0.7	0	1.0	0.2	2.0	3.2
	Tetrahydropyran	3.1	5.6	5.5	0.3	2.7	5.0
	2-Methyltetrahydrofuran	2.1	2.1	2.1	0.5	3.5	3.8
	Pentane-1,2-diol	1.5	0.7	2.6	7.8	5.0	3.1
	(Tetrahydrofuran-2-yl)methanol	11.1	0	5.3	2.9	10.2	12.2
C6	Hexanol	5.0	0.7	10.7	1.1	8.7	10.4
	Hexanone	0.8	0	1.3	1.1	8.9	3.7
	2,5-Dimethyltetrahydrofuran	1.2	0.8	1.0	0.6	1.8	1.0
	2-Methyltetrahydropyran	3.3	4.3	4.1	0.3	3.2	7.2
	Hexane-1,2-diol	0	0	0.7	1.4	0.5	0.8
	(Tetrahydropyran-2-yl)methanol	14.2	0.9	17.1	6.2	18.9	2.9
	Hexane-1,2,6-triol	0	0	0	0	0	0
	Isosorbide and 1,4-sorbitan	0	0	0	27.0	0	0
	Sorbitol	0	0	0	38.0	0	0
Carbon identified (mol%)		84.3	101.7	104.2	77.5	76.0	98.4

<sup>a</sup> Reaction condition: 2.93 MPa with 5 wt% sorbitol solution as the feed and H<sub>2</sub> flow rate of about 45 mL min<sup>-1</sup>.

conversion to the gas phase products went through a maximum at 3.48 MPa. The C5 and C6 selectivity in both the gas phase and the liquid phase increased with total pressure. In contrast, the C1 selectivity in both the gas phase (mainly composed of CO<sub>2</sub>) and the liquid phase (methanol) decreased with total pressure (*i.e.*, hydrogen concentration at the reactor inlet).

The liquid products were mainly alcohols. The yield of C1–C3 compounds decreased with increasing system pressure. The major C4–C6 compounds in the liquid phase were

alcohols and cyclic ethers at low initial hydrogen concentration. With the increase in initial hydrogen concentration, the yield of C4–C6 increased, and the major compounds changed from cyclic ethers to alcohols (butanol, pentanol, and hexanol).

**4.1.3. Effects of sorbitol feed concentration.** Table 3 shows the effect of sorbitol feed concentration on the catalytic performance of 4 wt% Pt/SiO<sub>2</sub>–Al<sub>2</sub>O<sub>3</sub> catalyst. As sorbitol feed concentration increased, the carbon conversion to the gas

**Table 2** Total molar carbon selectivity of products in gas- and liquid-phase as a function of pressure for the APHDO of sorbitol<sup>a</sup>

Data set number		2	8	9	10	11
Pressure (MPa)		2.93	3.48	4.17	4.9	5.65
Conversion (mol%)		100	100	100	100	100
Gas phase yield (mol%)		80.8	90.5	86.9	74.7	64.3
<b>Gas phase carbon selectivity (mol%)</b>						
C1	Carbon dioxide	40.4	26.3	24.6	19.4	18.3
	Methane	5.2	3.9	3.3	1.8	1.4
C2	Ethane	13.8	10.6	9.8	7.9	7.3
C3	Propane	9.7	9.1	9.3	10.3	10.8
C4	Butane	10.4	11.1	11.4	10.1	9.6
C5	Pentane	8.9	14.5	14.7	16.1	17.8
C6	Hexane	11.6	24.6	26.8	34.5	34.8
<b>Liquid phase yield (mol%)</b>						
C1		2.1	1.3	1.3	0.8	0.7
C2		5.7	3.0	4.8	4.9	4.6
C3		8.8	4.1	6.9	11.0	12.2
C4		1.0	0.3	0.7	2.5	3.7
C5		1.9	0.8	1.1	3.7	6.4
C6		1.4	0.5	0.9	7.1	16.9
<b>Liquid phase carbon selectivity (mol%)</b>						
C1	Methanol	9.9	13.4	8.6	2.8	1.5
C2	Ethanol	27.5	30.0	30.7	16.4	10.3
C3	Propanol	40.3	40.9	44.2	36.5	27.5
	Acetone	0.9	0	0	0	0
	Glycol	0	0	0	0	0
	Propane-1,2-diol	1.0	0	0	0	0
	1-Hydroxypropan-2-one	0	0	0	0	0
	Glycerol	0	0	0	0	0
C4	Butanol	4.6	2.9	4.2	8.5	8.2
	Butanone	0	0	0	0	0
	Tetrahydrofuran	0	0	0	0	0
	Butanediol	0	0	0	0	0
C5	Pentanol	0.8	2.7	3.4	6.7	7.9
	Pentanone	0	0	0	0	0
	Tetrahydropyran	5.6	5.4	3.3	3.0	2.4
	2-Methyltetrahydrofuran	2.1	0	0	0	2.1
	Pentane-1,2-diol	0.7	0	0	1.1	0
	(Tetrahydrofuran-2-yl)methanol	0	0	0	1.4	2.1
C6	Hexanol	0.7	1.4	2.4	15.4	28.5
	Hexanone	0	0	0	1.3	3.9
	2,5-Dimethyltetrahydrofuran	0.8	0	0	3.0	3.3
	2-Methyltetrahydropyran	4.3	3.3	3.2	3.8	1.4
	Hexane-1,2-diol	0	0	0	0	0
	(Tetrahydropyran-2-yl)methanol	0.9	0	0	0.2	0.8
	Hexane-1,2,6-triol	0	0	0	0	0
	Isosorbide and 1,4-sorbitan	0	0	0	0	0
	Sorbitol	0	0	0	0	0
Carbon identified (mol%)		101.7	100.5	102.6	104.8	108.8

<sup>a</sup> Reaction condition: 518 K, WHSV = 0.73 h<sup>-1</sup>, with 5 wt% sorbitol solution as the feed, and H<sub>2</sub> flow rate of about 45 mL min<sup>-1</sup>.

phase decreased. The C5 and C6 gas phase selectivity went through a maximum with respect to sorbitol feed concentration. As the sorbitol feed concentration increased from 10 to 50 wt%, the C1 gas phase selectivity increased and the C2–C6 gas phase selectivity decreased.

The increase in the sorbitol feed concentration increased the yield of C6 carbon that was in the liquid phase. At the highest sorbitol feed concentration, most of this carbon was present as isosorbide and unconverted sorbitol. The selectivities of

hexanol and hexanediol were maximized at a sorbitol feed concentration of 20 wt%.

In the liquid phase products, the yield of C1–C3 compounds went through a maximum around a sorbitol feed concentration of 10 wt%. The major C1–C3 product at a sorbitol feed concentration of 10 wt% to 50 wt% was propane-1,2-diol. At the lowest sorbitol feed concentration, the C1–C3 product selectivity favors primarily alcohols (selectivity sequence: propanol > ethanol > methanol).

**Table 3** Total molar carbon selectivity of products in gas- and liquid-phase as a function of sorbitol feed concentration for the APHDO of sorbitol<sup>a</sup>

Data set number	2	13	14	15
Sorbitol feed concentration (wt%)	5	10	20	50
Conversion (mol%)	100	100	100	79.0
Gas phase yield (mol%)	80.8	26.6	10.9	4.2
<b>Gas phase carbon selectivity (mol%)</b>				
C1 Carbon dioxide	40.4	30.2	52.4	75.8
Methane	5.2	1.8	2.6	2.0
C2 Ethane	13.8	6.4	7.5	2.4
C3 Propane	9.7	7.5	7.6	1.8
C4 Butane	10.4	7.0	5.7	3.8
C5 Pentane	8.9	14.0	9.5	5.3
C6 Hexane	11.6	33.2	14.7	8.9
Liquid phase yield (mol%)	20.9	86.8	60.2	85.2
C1	2.1	1.2	0.7	0.3
C2	5.7	3.5	1.8	0.6
C3	8.8	43.4	13.5	11.7
C4	1.0	19.8	15.1	4.3
C5	1.9	8.4	8.5	4.3
C6	1.4	10.5	20.8	64.0
<b>Liquid phase carbon selectivity (mol%)</b>				
C1 Methanol	9.9	1.4	1.1	0.4
C2 Ethanol	27.5	4.1	2.9	0.7
C3 Propanol	40.3	7.2	7.8	0.8
Acetone	0.9	0.4	0.5	0
Glycol	0	8.5	0	2.4
Propane-1,2-diol	1.0	32.6	13.1	7.0
1-Hydroxypropan-2-one	0	1.3	1.0	1.4
Glycerol	0	0	0	2.2
C4 Butanol	4.6	1.8	2.1	0.3
Butanone	0	7.9	13.4	0.5
Tetrahydrofuran	0	3.3	4.0	1.3
Butanediol	0	9.8	5.5	3.0
C5 Pentanone	0.8	2.1	2.7	0.7
Pentanone	0	0.5	1.5	0.6
Tetrahydropyran	5.6	0.6	0.8	0.2
2-Methyltetrahydrofuran	2.1	1.4	2.5	1.1
Pentane-1,2-diol	0.7	1.9	2.5	1.1
(Tetrahydrofuran-2-yl)methanol	0	3.3	4.0	1.3
C6 Hexanol	0.7	4.1	5.4	0.5
Hexanone	0	1.1	10.3	1.8
2,5-Dimethyltetrahydrofuran	0.8	1.7	3.6	0.9
2-Methyltetrahydropyran	4.3	0.2	0.8	0.2
Hexane-1,2-diol	0	3.1	4.9	2.3
(Tetrahydropyran-2-yl)methanol	0.9	0	2.0	0.6
Hexane-1,2,6-triol	0	1.6	3.7	0.5
Isosorbide and 1,4-sorbitan	0	0.3	3.7	48.7
Sorbitol	0	0	0	19.7
Carbon identified (mol%)	101.7	113.5	71.1	89.4

<sup>a</sup> Reaction condition: 518 K, 2.93 MPa, WHSV = 0.73 h<sup>-1</sup>, and H<sub>2</sub> flow rate of about 45 mL min<sup>-1</sup>.

The yield of C4–C5 liquid phase products also went through a maximum with respect to sorbitol feed concentration. At high sorbitol feed concentration, the major C4–C5 products were butanediol, butanone, and tetrahydrofuran compounds. No C4–C5 product contained more than two oxygen atoms. At the lowest sorbitol feed concentration, the selectivity sequence of C4–C5 products is tetrahydropyran > butanol > 2-methyltetrahydrofuran.

## 4.2. Reaction network statistics

The automatically generated network consists of 4804 irreversible chemical reactions in total. The reaction count for each individual reaction family is given in Table 4. The most prevalent reaction families are alcohol dehydration and pinacol rearrangement.

A total of 1178 distinct chemical species are included in the reaction network, while only three species (sorbitol, hydrogen, and water) were used for network generation. The maximum number of experimentally measured species (including positional isomers) in a given data set was 43. The complete reaction network and species list are available as ESI (Tables 9 and 10, respectively<sup>†</sup>).

## 4.3. Tuning of kinetic parameters

Each of the tuned kinetic rate parameters for all 20 of the reaction families is given in Table 5. The LFER given in eqn (2) is nontrivial only for the 17 reaction families with nonzero  $\alpha_i$  parameters. The remaining reaction families share a single rate constant ( $\log k_{0,i}$ ) for all reactions. With all  $E_{0,i}^*$  set to zero, there are a total of 37 kinetic parameters in this tuned model.

The relative rates of competing reaction pathways are shown by the values of the tuned kinetic parameters. The bifunctional catalyst promotes both dehydration (primarily on acid catalytic sites) and decarbonylation (primarily on metal catalytic sites), with a slightly faster rate of decarbonylation than alcohol dehydration (RF4 *versus* RF9). The rate constants for aldehyde hydrogenation and the opposing primary alcohol dehydrogenation reaction (RF6 and RF16) suggest that aldehydes do not readily convert into primary alcohols. The high rates of decarbonylation and water–gas shift (RF9 and RF20) lead to significant production of carbon dioxide *via* the consumption of aldehydes. The relative parameter values for RF10 and RF11 indicate that dihydrofuran rings saturate more readily than aromatic furan rings.

## 4.4. Parity plots

A parity plot of each data set used for parameter tuning is given in Fig. 3. Each plot compares the model prediction for the product composition to the experimentally measured product composition, with a diagonal line to indicate the ideal model fit. The parity plots for the data sets with the poorest fit are shown in Fig. 3a and d. These data sets are at the high and low ends of the pressure range used for parameter tuning. The data set with the worst model fit also deviated the most from 100 mol% identified carbon. The products with the lowest prediction accuracy are ethanol and propanol. Fig. 4 shows a parity plot with species labels to show the relative accuracy for these products. The accuracy of the model fit to the experimental data is summarized in Table 6.

Fig. 5 shows how the reaction pressure and identified carbon percentage affect the accuracy of the model predictions. The models were the most accurate (*i.e.*, had the highest coefficients of determination) for the data sets at the center of the pressure

**Table 4** Reaction count by reaction family

RF#	Reaction family	Count
RF1	Acyclic thermal cracking	12
RF2	Alcohol cyclization 5	68
RF3	Alcohol cyclization 6	30
RF4	Alcohol dehydration	958
RF5	Alcohol ring closure	6
RF6	Aldehyde hydrogenation	487
RF7	C–O hydrogenolysis 5	140
RF8	C–O hydrogenolysis 6	56
RF9	Decarbonylation	487
RF10	Furan ring saturation 2H	126
RF11	Furan ring saturation 4H	18
RF12	Hydrogenation ( <i>n</i> -olefin)	21
RF13	Hydrogenation (oxygenated species)	417
RF14	Ketone hydrogenation	491
RF15	Pinacol rearrangement	613
RF16	Primary alcohol dehydrogenation	487
RF17	Pyran ring saturation	167
RF18	Retro-aldol condensation	218
RF19	Reverse water–gas shift	1
RF20	Water–gas shift	1
	Total	4804

**Table 5** Tuned kinetic parameters of each reaction family.  $n$  ≡ reaction order,  $k_0$  ≡ rate constant ( $M^{1-n} s^{-1}$ ),  $\alpha$  ≡ LFER constant

RF#	Reaction family	$n$	$\log k_0$	$\alpha$
RF1	Acyclic thermal cracking	1	5.5	1.00
RF2	Alcohol cyclization 5	1	6.4	−0.12
RF3	Alcohol cyclization 6	1	7.1	0.01
RF4	Alcohol dehydration	1	7.3	−0.01
RF5	Alcohol ring closure	1	3.8	0.16
RF6	Aldehyde hydrogenation	2	5.7	0.04
RF7	C–O hydrogenolysis 5	2	11.8	1.00
RF8	C–O hydrogenolysis 6	2	11.4	1.00
RF9	Decarbonylation	1	7.8	0.07
RF10	Furan ring saturation 2H	2	8.1	0.09
RF11	Furan ring saturation 4H	3	4.5	−0.05
RF12	Hydrogenation ( <i>n</i> -olefin)	2	13.3	0.13
RF13	Hydrogenation (oxygenated species)	2	6.1	0.01
RF14	Ketone hydrogenation	2	6.2	−0.03
RF15	Pinacol rearrangement	1	7.2	0.00
RF16	Primary alcohol dehydrogenation	1	6.6	−0.06
RF17	Pyran ring saturation	2	7.9	0.22
RF18	Retro-aldol condensation	1	7.6	−0.01
RF19	Reverse water–gas shift	2	0.0	0.00
RF20	Water–gas shift	2	10.0	0.00

range (data sets 2, 8, 9, and 10; Fig. 5a). Model fit also suffers slightly as identified carbon deviates from 100 mol%, as shown in Fig. 5b.

## 5. Discussion

### 5.1. Effects of reaction conditions on target products

Hydrodeoxygenation of biomass-derived compounds produces a wide variety of species and is greatly influenced by reaction conditions. It is important to understand how reaction

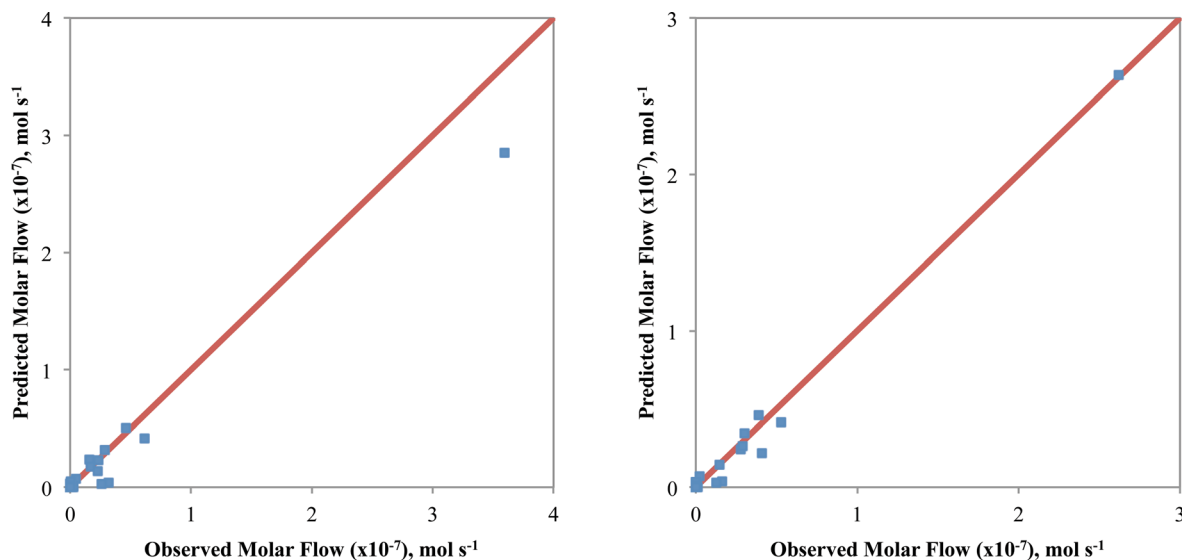
conditions, such as temperature, pressure, and feed concentration, can affect the reaction products. In this paper, we have shown how yield and/or selectivity to C5–C6 alkanes, C1–C3 alcohols and diols, and C4–C6 alcohols and diols change with reaction conditions. As we proposed previously,<sup>16</sup> another promising application of APHDO of sorbitol is the production of low-oxygen-content species or monofunctional compounds.<sup>11</sup> Some of these compounds, including 2-methyltetrahydrofuran and 2,5-dimethyltetrahydrofuran, can be directly used as fuels or fuel additives.<sup>36</sup>

C4–C6 alcohols, ketones, and diols can be used to produce liquid fuels by aldol condensation followed by aqueous-phase hydrodeoxygenation.<sup>11</sup> The selectivity of C4–C6 alcohols and diols increases with increasing pressure and goes through a maximum with respect to temperature (at WHSV = 2.91 h<sup>−1</sup>) and sorbitol feed concentration. The C4–C6 products are formed *via* a series of reaction pathways from sorbitol. These C4–C6 products are then converted into C4–C6 alkanes, C1–C3 oxygenates, or C1–C3 alkanes and CO<sub>2</sub>. Increasing the sorbitol feed concentration decreases the overall sorbitol conversion (see Table 3), which in turn decreases the yield of C4–C6 alcohols and diols.

Cyclic ether intermediates (such as isosorbide) are generated by the dehydration of sorbitol. These products have a low rate of C–C bond cleavage and can selectively produce large amounts of C5 and C6 alkanes.<sup>16</sup> The C5–C6 alkanes could be isomerized and added into gasoline. The yield of C5–C6 alkanes increases with increasing temperature at higher WHSV. This increase results from the conversion of C5–C6 alcohols and diols into alkanes. The yield of C5–C6 alkanes also increases dramatically as the pressure increases from 2.93 to 3.48 MPa. After a further increase in pressure, the C5–C6 yield does not continue to increase. The maximum in the gasoline-range (C5 and C6 normal alkanes) product yield with respect to sorbitol feed concentration results from the decrease in water concentration with increased sorbitol concentration, which encourages the dehydration of sorbitol. The comparable selectivity of C1–C4 light alkanes at similar gas phase carbon conversion implies that the reaction pathway does not significantly change with temperature.

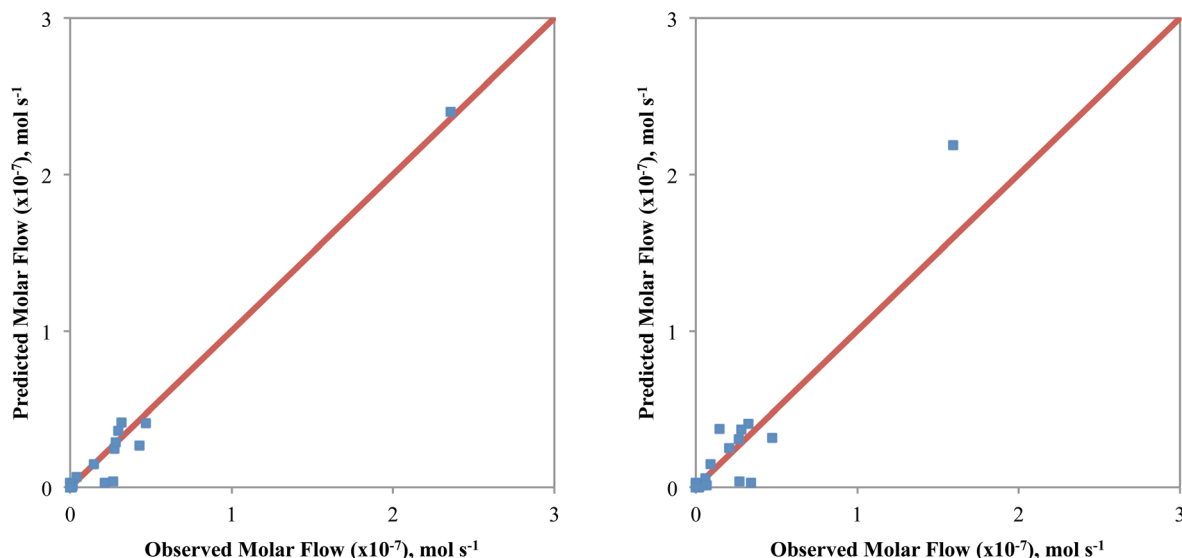
C1–C3 alcohols and diols are valuable commodity chemicals that have functional value beyond their fuel value. The highest C1–C3 yield was achieved at 518 K, 2.93 MPa, and WHSV = 0.73 h<sup>−1</sup> with 10 wt% of sorbitol as the feed. Combined with the observations for C4–C6 alcohols and diols, these conditions appear to be optimal for alcohol and diol production. The selectivity of C1–C3 alcohols and diols increases with reaction temperature.

The change in hydrogen concentration resulting from reaction pressure has a drastic effect on the product selectivity for the APHDO of sorbitol. The hydrogen concentration can be used to adjust the relative rates of C–C *versus* C–O bond cleavage. The decrease in C1 product selectivity with increasing total pressure is most likely due to an increase in hydrogen partial pressure. Increasing the system pressure increases the hydrogen concentration and most likely results in a decrease in the rate of dehydrogenation, which is the first step in C–C bond cleavage



a. Data Set 2,  $x_0 = 5$  wt%,  $P = 2.93$  MPa,  $T = 518$  K,  $\text{WHSV} = 0.73 \text{ hr}^{-1}$ ,  $y = 101.7$  mol%,  $F = 0.751$ ,  $R^2 = 0.913$

b. Data Set 8,  $x_0 = 5$  wt%,  $P = 3.48$  MPa,  $T = 518$  K,  $\text{WHSV} = 0.73 \text{ hr}^{-1}$ ,  $y = 100.5$  mol%,  $F = 0.0902$ ,  $R^2 = 0.987$



c. Data Set 9,  $x_0 = 5$  wt%,  $P = 4.17$  MPa,  $T = 518$  K,  $\text{WHSV} = 0.73 \text{ hr}^{-1}$ ,  $y = 102.6$  mol%,  $F = 0.136$ ,  $R^2 = 0.977$

d. Data Set 10,  $x_0 = 5$  wt%,  $P = 4.90$  MPa,  $T = 518$  K,  $\text{WHSV} = 0.73 \text{ hr}^{-1}$ ,  $y = 104.6$  mol%,  $F = 0.609$ ,  $R^2 = 0.873$

**Fig. 3** Parity plots: predicted molar flow versus observed molar flow ( $\times 10^{-7}$ ),  $\text{mol s}^{-1}$ .  $x_0 \equiv$  sorbitol feed concentration (wt%),  $P \equiv$  pressure (MPa),  $T \equiv$  temperature (K),  $\text{WHSV} \equiv$  weight hourly space velocity ( $\text{h}^{-1}$ ),  $y \equiv$  carbon identified in measured products (mol%),  $F \equiv$  objective function value,  $R^2 \equiv$  coefficient of determination.

by decarbonylation.<sup>16</sup> Therefore, higher hydrogen concentration inhibits decarbonylation.

The shift in gas phase selectivity from C2–C6 to C1 with increasing sorbitol feed concentration occurs primarily because more carbon is cleaved *via* decarbonylation to CO, followed by immediate conversion to CO<sub>2</sub> *via* water–gas shift. We have previously shown that the C1 gas phase selectivity increases as the WHSV increases and that most of the C1 gas phase products are formed from decarbonylation reactions.<sup>16</sup> The low oxygen content (two oxygen atoms or fewer) of C4–C5 products at high sorbitol feed concentration indicates that

these products were primarily formed *via* decarbonylation reactions.

Propane-1,2-diol and glycerol are most likely formed by retro-aldol condensation of sorbitol. The alcohols are formed by hydrodeoxygenation of propane-1,2-diol and glycerol or from decarbonylation of larger oxygenates. The smaller increase in gas phase yield with increasing reaction temperature at low WHSV can be explained because carbon conversion to the gas phase at low WHSV is very high (>80 mol%). As a result, the oxygenate concentration in the solution was lower and the effect of temperature became less evident. The high selectivity of

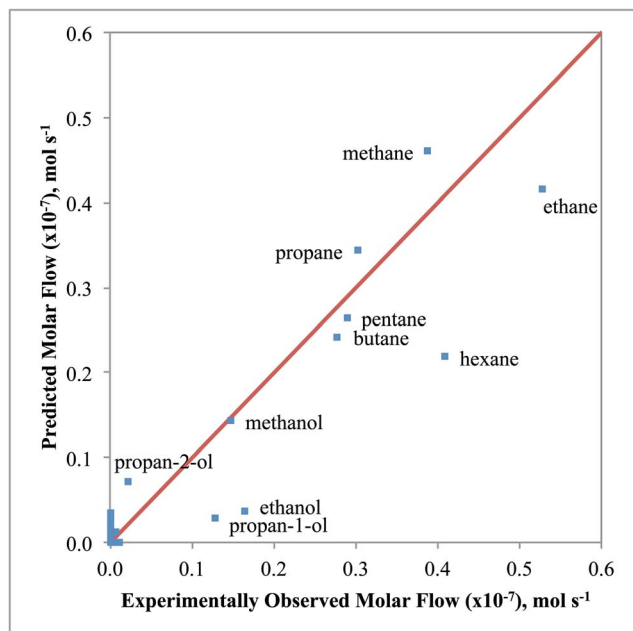


**Fig. 4** Parity plot detail with selected species labels. For clarity, this scale does not show carbon dioxide or any species with observed molar flow rates less than  $1 \times 10^{-9} \text{ mol s}^{-1}$ . Data Set 8,  $x_0 = 5 \text{ wt\%}$ ,  $P = 3.48 \text{ MPa}$ ,  $T = 518 \text{ K}$ ,  $\text{WHSV} = 0.73 \text{ h}^{-1}$ ,  $y = 100.5 \text{ mol\%}$ ,  $F = 0.0902$ ,  $R^2 = 0.987$ .

C1–C3 alcohols and diols is in accordance with the pathway we assumed for the retro-aldol condensation of sorbitol in our previous work.<sup>16</sup> Table 7 summarizes the effects that the reaction conditions have on the selectivities of each species type in this system.

In practical applications, we can choose the proper reaction conditions depending upon which products are desired. At higher pressure, for example, we can selectively produce pentane and hexane, which can be used to produce gasoline with a high octane value by hydroisomerization. Likewise, we can also selectively produce alcohols to make C1–C3 low-oxygen-content compounds for the production of hydrogen or make C4–C5 low-oxygen-content for liquid, jet-fuel-range, large, normal alkanes by dehydrogenation and aldol condensation of alcohols followed by aqueous phase hydrodeoxygenation.

The current work mainly focuses on the effect of sorbitol feed concentration. In the future, further detailed work on the effect of concentration of reaction intermediates are still needed to provide deeper insight into how to control the selectivity for these series-parallel reaction networks.

## 5.2. Model fit

The model fits are most accurate for the data sets that were used for parameter tuning. As expected, weaknesses in the predictive abilities of the kinetic model became more pronounced at conditions that varied significantly from those at which the model was tuned. Since the data were tuned using all of the varied pressure data sets (except for the highest pressure because of the high identified carbon percentage), Fig. 5a is a smooth curve with a central maximum.

All of the experimental data were at 100 mol% sorbitol conversion, except for data sets 4 and 15 (which were at 74.6 mol% and 79.0 mol%, respectively). Those data sets have low identified carbon percentages that did not allow for reliable parameter tuning. Due to a lack of low conversion data, a kinetic study to identify the reaction intermediates proved challenging.

Data sets 2, 8, 9, and 10, which were used for parameter tuning, have identical sorbitol feed concentration (5 wt%), temperature (518 K), WHSV ( $0.73 \text{ h}^{-1}$ ), and identified carbon balances near 100 mol%, while they differ only in system pressure (2.93, 3.48, 4.17, and 4.90 MPa, respectively). Temperature dependence could not be included in the rate parameters for this model because there were an insufficient number of data sets with near-100 mol% identified carbon at varied temperature (with all other conditions constant). Therefore, we could not effectively deduce the  $\log A_{0,i}$  and  $E_{0,i}^*$  values and instead utilized a  $\log k_{0,i}$  value. As a result of the temperature-independent rate parameters, accurate predictions cannot be made at varied temperatures.

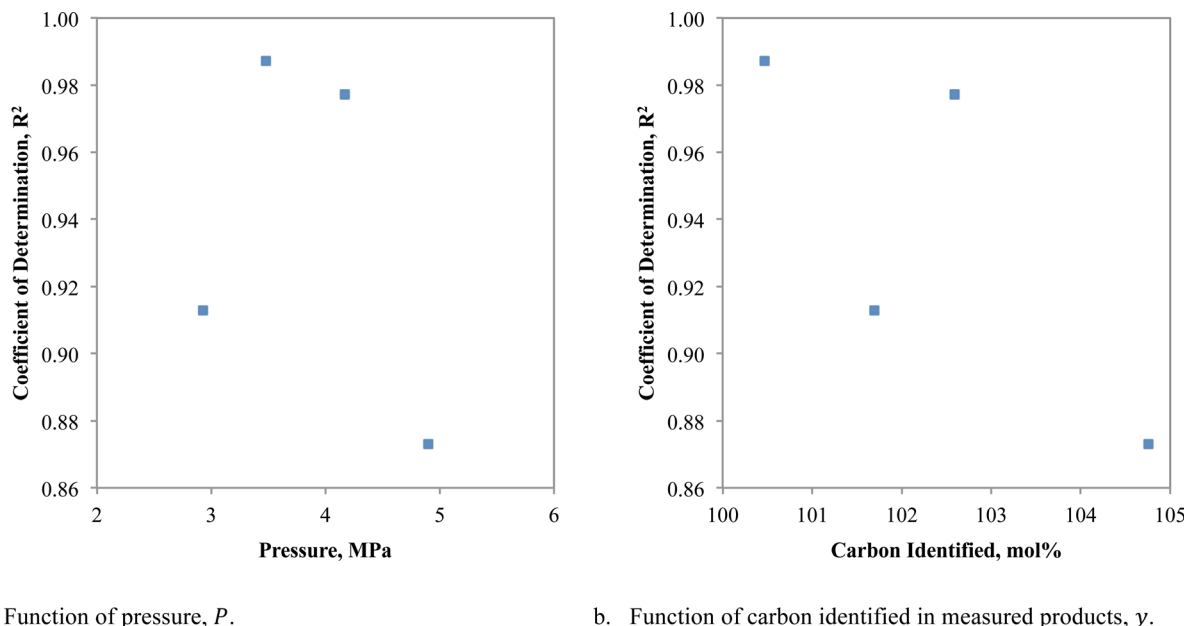
A requirement for accurate kinetic modeling is complete product identification. If an insufficient (or extraneous) percentage of products are measured, the numerical predictions of the kinetic model will overestimate (or underestimate) the experimental results. Most of the data sets with low coefficients of determination also have identified carbon percentages that differ significantly from 100 mol%.

The tuned kinetic rate parameters for competing reactions indicate which reaction pathway controls the production of a given species. For example, the rate constants for alcohol dehydration and decarbonylation are very similar, which indicates that these two deoxygenation methods are approximately equally dominant at the tuned conditions. Balanced data at various reaction temperatures would enable tuning of the activation energies for each of the reaction families in this model. Knowing the activation energies of competing reaction pathways can help to direct catalyst research by modulating between these pathways to favor desired products.

Within the constraints of this tuned kinetic model, we can identify reaction intermediates and compare rate constants for competing reactions. Given additional data with approximately 100 mol% identified carbon at varied conditions, we could obtain more detailed information about the specific effects of reaction conditions on intermediate species and pathways.

**Table 6** Summary of model fit.  $x_0 \equiv$  sorbitol feed concentration (wt%),  $P \equiv$  pressure (MPa),  $T \equiv$  temperature (K),  $\text{WHSV} \equiv$  weight hourly space velocity ( $\text{h}^{-1}$ ),  $y \equiv$  carbon identified in measured products (mol%),  $F \equiv$  objective function value,  $R^2 \equiv$  coefficient of determination

Fig. 3	Data set	$x_0$ (wt%)	$P$ (MPa)	$T$ (K)	WHSV ( $\text{h}^{-1}$ )	$y$ (mol%)	$F$	$R^2$
a	2	5	2.93	518	0.73	101.7	0.751	0.913
b	8	5	3.48	518	0.73	100.5	0.0902	0.987
c	9	5	4.17	518	0.73	102.6	0.136	0.977
d	10	5	4.90	518	0.73	104.8	0.609	0.873

a. Function of pressure,  $P$ .b. Function of carbon identified in measured products,  $y$ .**Fig. 5** Coefficient of determination as a function of reaction conditions.  $x_0 = 5$  wt%,  $T = 518$  K,  $WHSV = 0.73$  h<sup>-1</sup>, varied pressure.**Table 7** Summary of the effect of reaction conditions on species type selectivity.  $x_0$   $\equiv$  sorbitol feed concentration (wt%),  $P$   $\equiv$  pressure (MPa),  $T$   $\equiv$  temperature (K),  $WHSV$   $\equiv$  weight hourly space velocity (h<sup>-1</sup>). High or low values of each reaction condition maximize or minimize the selectivity of each species type. Rank refers to the minimum number of reaction steps from sorbitol; in this case, low rank species are intermediates. Selectivity trends with temperature also depend upon weight hourly space velocity

Species type	Sorbitol, $x_0$		Pressure, $P$		Temperature, $T$		WHSV	
	Max	Min	Max	Min	Max	Min	Max	Min
Carbon dioxide	Low $x_0$	High $x_0$	Low $P$	High $P$	High $T$	Low $T$	Low WHSV	High WHSV
Alkane, C1–C5	Low $x_0$	High $x_0$	Low $P$	High $P$	High $T$	Low $T$	Low WHSV	High WHSV
Hexane	Low $x_0$	High $x_0$	High $P$	Low $P$	High $T$	Low $T$	Low WHSV	High WHSV
Methanol	Low $x_0$	High $x_0$	Low $P$	High $P$	High $T$	Low $T$	Low WHSV	High WHSV
Primary alcohol, C2–C6	Low $x_0$	High $x_0$	High $P$	Low $P$	High $T$	Low $T$	Low WHSV	High WHSV
Secondary alcohol	Low $x_0$	High $x_0$	High $P$	Low $P$	Low $T$	High $T$	Low WHSV	High WHSV
Diol	Low $x_0$	High $x_0$	N/A	N/A	Low $T$	High $T$	High WHSV	Low WHSV
Triol	Low $x_0$	High $x_0$	N/A	N/A	Low $T$	High $T$	High WHSV	Low WHSV
Ketone	20 wt%	Otherwise	High $P$	Low $P$	High $T$ & high WHSV	Low $T$ & high WHSV	High WHSV	Low WHSV
					Low $T$ & low WHSV	High $T$ & low WHSV		
Furan, low rank	High $x_0$	Low $x_0$	High $P$	Low $P$	High $T$ & high WHSV	Low $T$ & high WHSV	High WHSV	Low WHSV
					Low $T$ & low WHSV	High $T$ & low WHSV		
Furan, high rank	Low $x_0$	High $x_0$	High $P$	Low $P$	High $T$ & high WHSV	Low $T$ & high WHSV	High WHSV	Low WHSV
					Low $T$ & low WHSV	High $T$ & low WHSV		
Pyran	20 wt%	Otherwise	High $P$	Low $P$	High $T$ & high WHSV	Low $T$ & high WHSV	Low WHSV	High WHSV
					Low $T$ & low WHSV	High $T$ & low WHSV		

## 6. Conclusions

We investigated the effect of temperature, pressure, and sorbitol feed concentration on the aqueous phase hydrodeoxygenation (APHDO) of sorbitol over a 4 wt% Pt/SiO<sub>2</sub>-Al<sub>2</sub>O<sub>3</sub> catalyst. Deoxygenation is necessary for the production of valuable products such as fuels from biomass derivatives. Specifically, hydrodeoxygenation is desirable because the oxygen can be removed by the addition of hydrogen while maintaining the carbon number. APHDO of sorbitol results in a wide variety of products including liquid alkanes, light alkanes,

alcohols, and polyols. Changes in the reaction conditions control the product selectivity.

We constructed a complete reaction network for sorbitol hydrodeoxygenation that produces all experimentally measured species. All of the kinetic balance equations were automatically generated and parameter tuning was constrained *via* reaction families for a simplified solution. The kinetic model predictions are in very good agreement with the experimental results.

The completed kinetic model enables the prediction of product composition for varying feed composition and experimental conditions, determination of optimal conditions,

identification of the major and minor pathways and intermediate species, as well as the potential to identify the most suitable feedstock composition to obtain a desired product, all of which increase energy efficiency and reduce consumption of resources.

The reaction pathway and kinetic rate information that is captured in this model can be used to make predictions about more realistic feedstocks including cellulose by describing the secondary reactions following cellulose depolymerization. Sorbitol is a hydrogenation product of glucose, which is the monomeric unit of cellulose. Since both glucose and sorbitol are intermediate species in the conversion of cellulose to small molecules, the kinetic model presented in this paper describes the chemical reactions that occur after the initial depolymerization of the cellulose macromolecule.

Further understanding of this reaction chemistry combined with catalyst improvements will lead to targeted product selectivity from the hydrodeoxygenation of biomass-derived feedstocks. Results will be used to direct further experimentation and utilization of sorbitol as a surrogate molecule for biomass-to-fuels processing. Given more complete data, this model could direct catalyst research to modulate desired deoxygenation pathways *via* tuned activation energy and identify the reaction conditions that will make biofuels a competitive energy source.

## Notation

$k_j$	Rate constant of reaction $j$ , $M^{1-n} s^{-1}$
$k_{0,i}$	Rate constant of reaction family $i$ , $M^{1-n} s^{-1}$
$E_j^*$	Activation energy of reaction $j$ , $\text{kJ mol}^{-1}$
$E_{0,i}^*$	Activation energy of reaction family $i$ , $\text{kJ mol}^{-1}$
$F$	Sum of squares of residuals objective function value
$n$	Reaction order
$P$	Absolute pressure, MPa
$R$	Universal gas constant, $\text{cm}^3 \text{MPa mol}^{-1} \text{K}^{-1}$
$R^2$	Coefficient of determination
$T$	Absolute temperature, K
$x_0$	Sorbitol feed concentration, wt%
$y$	Carbon identified in measured products, mol%

## Greek letters

$\alpha_i$	LFER constant of reaction family $i$
$\Delta H_{R,j}$	Enthalpy change of reaction $j$ , $\text{kJ mol}^{-1}$

## Abbreviations

APHDO	Aqueous-phase hydrodeoxygenation
CME	Composition Modeling Editor
INGen	Interactive Network Generator
KME	Kinetic Modeling Editor
KMT	Kinetic Modeling Toolkit
LFER	Linear free energy relationship
RF#	Reaction family #
WHSV	Weight hourly space velocity, $\text{h}^{-1}$

## References

- 1 L. Lynd, M. Laser, D. Brandsby, B. Dale, B. Davison, R. Hamilton, M. Himmel, M. Keller, J. McMillan, J. Sheehan and C. Wyman, *Nat. Biotechnol.*, 2008, **26**(2), 169–172.
- 2 A. Carroll and C. Somerville, *Annu. Rev. Plant Biol.*, 2009, **60**, 165–182.
- 3 J. R. Regalbuto, *Science*, 2009, **325**(5942), 822–824.
- 4 S. Brethauer and C. E. Wyman, *Bioresour. Technol.*, 2010, **101**(13), 4862–4874.
- 5 S. Chundawat, G. Beckham, M. Himmel and B. Dale, *Annu. Rev. Chem. Biomol. Eng.*, 2011, **2**, 121–145.
- 6 G. Huber, S. Iborra and A. Corma, *Chem. Rev.*, 2006, **106**(9), 4044–4098.
- 7 J. N. Chheda, G. W. Huber and J. A. Dumesic, *Angew. Chem., Int. Ed.*, 2007, **46**(38), 7164–7183.
- 8 D. M. Alonso, J. Q. Bond and J. A. Dumesic, *Green Chem.*, 2010, **12**(9), 1493–1513.
- 9 G. W. Huber, R. D. Cortright and J. A. Dumesic, *Angew. Chem., Int. Ed.*, 2004, **43**(12), 1549–1551.
- 10 G. W. Huber, J. N. Chheda, C. J. Barrett and J. A. Dumesic, *Science*, 2005, **308**(5727), 1446–1450.
- 11 E. L. Kunkes, D. A. Simonetti, R. M. West, J. C. Serrano-Ruiz, C. A. Gärtner and J. A. Dumesic, *Science*, 2008, **322**(5900), 417–421.
- 12 T. P. Vispute and G. W. Huber, *Green Chem.*, 2009, **11**(9), 1433–1445.
- 13 R. M. West, M. H. Tucker, D. J. Braden and J. A. Dumesic, *Catal. Commun.*, 2009, **10**(13), 1743–1746.
- 14 N. Li, G. A. Tompsett and G. W. Huber, *ChemSusChem*, 2010, **3**(10), 1154–1157.
- 15 N. Li, G. A. Tompsett, T. Zhang, J. Shi, C. E. Wyman and G. W. Huber, *Green Chem.*, 2011, **13**(1), 91–101.
- 16 N. Li and G. W. Huber, *J. Catal.*, 2010, **270**(1), 48–59.
- 17 R. Xing, A. V. Subrahmanyam, H. Olcay, W. Qi, G. P. Walsum, H. Pendse and G. W. Huber, *Green Chem.*, 2010, **12**(11), 1933–1946.
- 18 R. M. West, E. L. Kunkes, D. A. Simonetti and J. A. Dumesic, *Catal. Today*, 2009, **147**(2), 115–125.
- 19 R. M. West, Z. Y. Liu, M. Peter and J. A. Dumesic, *ChemSusChem*, 2008, **1**(5), 417–424.
- 20 C. Zhao, J. He, A. A. Lemonidou, X. Li and J. A. Lercher, *J. Catal.*, 2011, **280**(1), 8–16.
- 21 W. Xu, S. J. Miller, P. K. Agrawal and C. W. Jones, *ChemSusChem*, 2012, **5**(4), 667–675.
- 22 C. Zhao, Y. Kou, A. A. Lemonidou, X. Li and J. A. Lercher, *Angew. Chem.*, 2009, **121**(22), 4047–4050.
- 23 G. W. Huber, J. W. Shabaker, S. T. Evans and J. A. Dumesic, *Appl. Catal., B*, 2006, **62**(3–4), 226–235.
- 24 R. R. Davda, J. W. Shabaker, G. W. Huber, R. D. Cortright and J. A. Dumesic, *Appl. Catal., B*, 2003, **43**(1), 13–26.
- 25 J. W. Shabaker, G. W. Huber, R. R. Davda, R. D. Cortright and J. A. Dumesic, *Catal. Lett.*, 2003, **88**(1–2), 1–8.
- 26 E. I. Gürbüz, E. L. Kunkes and J. A. Dumesic, *Green Chem.*, 2010, **12**(2), 223–227.
- 27 M. Vasiliiu, K. Guynn and D. A. Dixon, *J. Phys. Chem. C*, 2011, **115**(31), 15686–15702.

- 28 T. P. Vispute, H. Zhang, A. Sanna, R. Xiao and G. W. Huber, *Science*, 2010, **330**(6008), 1222–1227.
- 29 Z. He and X. Wang, *Catalysis for Sustainable Energy*, 2012, **1**, 28–52.
- 30 C. A. Bennett, User-controlled kinetic network generation with INGen, PhD Dissertation, Chemical & Biochemical Engineering, Rutgers University, 2009.
- 31 I. Bucsí, Á. Molnár, M. Bartók and G. A. Olah, *Tetrahedron*, 1994, **50**(27), 8195–8202.
- 32 I. Bucsí, Á. Molnár, M. Bartók and G. A. Olah, *Tetrahedron*, 1995, **51**(11), 3319–3326.
- 33 W. Wei, C. A. Bennett, R. Tanaka, G. Hou, M. T. Klein, Jr and M. T. Klein, *Fuel Process. Technol.*, 2008, **89**(4), 350–363.
- 34 M. Boudart, *Kinetics of Chemical Processes*, Prentice-Hall, Inc., Englewood Cliffs, NJ, 1968.
- 35 Z. Hou, Software tools for molecule-based kinetic modeling of complex systems, PhD Dissertation, Chemical & Biochemical Engineering, Rutgers University, 2011.
- 36 Y. Román-Leshkov, C. J. Barrett, Z. Y. Liu and J. A. Dumesic, *Nature*, 2007, **447**(7147), 982–985.